This article was downloaded by:[University of Pennsylvania]
[University of Pennsylvania]
On: 17 January 2007
Access Details: [subscription number 731702704]
Publisher: Taylor & Francis
Informa Ltd Registered in England and Wales Registered Number: 1072954
Registered office: Mortimer House, 37-41 Mortimer Street, London W1T 3JH, UK

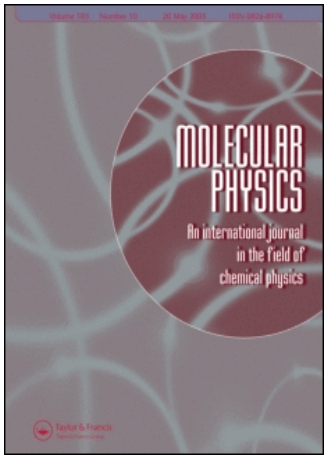

Molecular Physics
An International Journal in the Field of Chemical Physics
Publication details, including instructions for authors and subscription information:
http://www.informaworld.com/smpp/title~content=t713395160

"KMC-TDGL" - a coarse-grained methodology for simulating interfacial dynamics in complex fluids: application to protein-mediated membrane processes

To link to this article: DOI: 10.1080/00268970600997580
URL: http://dx.doi.org/10.1080/00268970600997580

Full terms and conditions of use: http://www.informaworld.com/terms-and-conditions-of-access.pdf
This article maybe used for research, teaching and private study purposes. Any substantial or systematic reproduction, re-distribution, re-selling, loan or sub-licensing, systematic supply or distribution in any form to anyone is expressly forbidden.
The publisher does not give any warranty express or implied or make any representation that the contents will be complete or accurate or up to date. The accuracy of any instructions, formulae and drug doses should be independently verified with primary sources. The publisher shall not be liable for any loss, actions, claims, proceedings, demand or costs or damages whatsoever or howsoever caused arising directly or indirectly in connection with or arising out of the use of this material.
© Taylor and Francis 2007

Molecular Physics, Vol. 104, Nos. 22–24, 20 November–20 December 2006, 3653–3666

Taylor & Francis
Taylor & Francis Group

'KMC-TDGL'—a coarse-grained methodology for simulating interfacial dynamics in complex fluids: application to protein-mediated membrane processes

J. WEINSTEIN† and R. RADHAKRISHNAN*

Department of Bioengineering, University of Pennsylvania, 240 Skirkanich Hall, 210 S. 33rd Street, Philadelphia PA 19104, USA

(*Received 31 July 2006; in final form 2 September 2006*)

In this article, we describe a new multiscale simulation algorithm (which we term the 'KMC-TDGL' method) applicable for the description of equilibrium and dynamic processes associated with a particular class of complex fluids with nanoscale inclusions, namely, biological membranes mediated by membrane-associating and membrane-bound proteins. We adopt a novel strategy of integrating two different phenomenological approaches, namely, a field theoretic (continuum) description for the membrane dynamics given by the time-dependent Ginzburg–Landau equation and a random walk on a discretized lattice description for protein diffusion dynamics. We illustrate that this integrated approach results in a unified description of protein-mediated membrane dynamics.

Downloaded By: [University of Pennsylvania] At: 17:48 17 January 2007

1. Introduction

Quantitative description of the thermodynamic and kinetic processes associated with membranes [1–5] has been an important research component in the physics of amphiphilic systems [6]. Several pioneering theoretical and modelling treatments have focused on different length and time-scales in order to probe the physical–chemical behaviour of membrane processes. Atomic-level simulations as well as coarse-grained models and simulations [7–15] have been successful in delineating the nature of specific interactions between membrane-bound proteins, molecules such as cholesterol and the membrane phase [7], in describing the pathways of micelle formation and vesicle fusion [16, 17], and in characterizing the elastic properties of membranes based on molecular interactions [18]. Phenomenological theories based on generalized elasticity (Ginzburg–Landau type) [4, 16, 19] have been used to describe the long time (meso and macroscopic) behaviour associated with membranes [20–22], undulations and curvature modulations in multi-component amphiphilic systems [23–25]. Monte Carlo simulations derived from these phenomenological models have also been successful in describing phase transitions, phase behaviour, budding phenomenon associated with multi-component vesicles [26], and protein mobility on membranes [27]. Phase separation and global thermodynamic phase behaviour in multi-component membranes have also been described by a combination of mean-field models and experiments involving vesicles [28–30, 31].

Despite this success in quantifying membrane phase behaviour, describing several biological processes in membranes mediated by proteins such as formation of caveolae (flask shaped vesicular structures formed in the membrane) [32, 33] or endocytotic vesicles (cell membrane invagination and vesicle formation regulated by membrane bound proteins) [34] has remained a challenge because these processes are cooperative and manifest at the mesoscale ($\sim\mu$m, $\sim$ms) even though the underlying interactions occur at the nanoscale. Therefore, a quantitative description of these underlying processes is inherently a multiscale problem. Study of such processes is of value from fundamental as well as applied aspects, as the interface between nanotechnology and biotechnology is rapidly evolving.

The field of multiscale modelling has a broad aim of quantitatively describing the interplay between processes at disparate length and time-scales (from Å to m and from fs to s) in order to predict molecular, mesoscopic, as well as macroscopic properties [35, 36]. The basic

*Corresponding author. Email: rradhak@seas.upenn.edu
†Current Address: Department of Bioengineering, Stanford University, USA.

Molecular Physics
ISSN 0026–8976 print/ISSN 1362–3028 online © 2006 Taylor & Francis
http://www.tandf.co.uk/journals
DOI: 10.1080/00268970600997580

components of multiscale modelling involve different modelling methods to describe the processes at different scales: *ab initio* methods for the electronic scale, molecular dynamics for the nanoscale, lattice Boltzmann for the mesoscale etc., as well as, different strategies for rationally bridging the scales (e.g. mixed quantum mechanics molecular mechanics for bridging electronic and nanoscopic scales). This latter aspect of multiscale modelling is very much in development; strategies employed for bridging the scales tend to be problem and context specific. A widely employed multiscale bridging strategy is based on coarse graining of the Hamiltonian or the energy function in order to reduce the number of degrees of freedom to be considered and in order to filter high frequency (shorter time-scale) modes [2, 14, 15, 36, 37]. More recently, a versatile class of hybrid methods has come into existence that combines different phenomenological theories or models. These methods are termed heterogeneous multiscale methods [35]. Heterogeneous multiscale methods are particularly adaptable in many complex scenarios where traditional multiscale approaches have their shortcomings and hence provide avenues to rationally bridge across disparate length and time-scales [36].

Transport of extracellular components into the cell via an internalization mechanism known as endocytosis is well appreciated in receptor regulation, neurotransmission and drug delivery. In this process, extracellular ligands bind and activate specific receptors and trigger diverse signalling events including plasma membrane invagination with the aid of several proteins, vesicle formation, and subsequently receptor internalization. While the signal transduction regulating endocytosis in cells is a complex and tightly regulated process [34], cell biology studies have determined that the receptor-mediated endocytosis occurs primarily through the interaction of epsin with the membrane, resulting in the induction of curvature in the membrane. However very little insight on how the collective interactions of epsins with the membrane lead to the origin of vesicle formation is obtained [39].

Motivated by this question, and inspired by the success of heterogeneous multiscale methods in different contexts, we build on this ideology and develop a new heterogeneous multiscale approach (the KMC-TDGL method) for studying membrane dynamical processes by combining two different phenomenological theories. In our multiscale spatially resolved stochastic model, we treat the membrane dynamics as a field evolving in time according to the time-dependent Ginzburg–Landau (TDGL) equation [4, 40]. We treat the diffusion of intracellular and membrane-bound proteins using a random walk process on a lattice using the kinetic Monte Carlo (KMC) approach [41]. In our integrated KMC-TDGL method, we combine the two descriptions using a methodology that is dictated by the competition between the time-scale of diffusion to that of membrane dynamics. We illustrate the application of this approach by studying protein mediated dynamical processes in membranes.

2. Models and methods

The biological complexity of protein–membrane interaction and the coupling to rheological and transport properties of membranes forbids the formulation of a theory and modelling strategy that incorporates all of the known details from structural biology at the atomic level. Our strategy here is to develop an approach by including crucial but manageable models of interactions at the mesoscale. Therefore simplifications and model approximations are an inevitable part of our computational strategy. We note that the specfic choice for the form and parameters of the interactions can be validated and independently determined by atomistic simulations and experiments (section 4).

2.1. *Protein–protein interaction*

Our system consists of proteins of a single kind (modelled after epsin) diffusing on and off the bilayer membrane (figure 1(a)). We have employed pre-validated phenomenological models of interactions, namely, protein diffusion is treated as a random walk on a lattice and the membrane is treated as an elastic continuum. Protein–protein interactions are limited to size exclusion (repulsive interactions on the scale of size of the protein, depicted in figure 1(b) as hard-sphere exclusion), and specific interactions between proteins are not considered consistent with experimental findings for epsin [39]. The parameters for exclusion are obtained from crystallographic data.

2.2. *Protein diffusion*

Our model includes protein diffusion in a probabilistic manner, i.e. hopping between discrete 'lattice' sites. The density of proteins adsorbed on the membrane is denoted by the unitless surface density,

$$\rho^* = \frac{N^{\text{adsorbed}} \times a_0^2}{A},$$

where a_0 is lattice length, ρ^* is reduced surface density, N^{adsorbed} is the number of adsorbed proteins and A is the total area. We explicitly allow for the diffusion of the proteins in the extracellular, intracellular and membrane-bound phases. The diffusion is treated via a

Downloaded By: [University of Pennsylvania] At: 17:48 17 January 2007

Downloaded By: [University of Pennsylvania] At: 17:48 17 January 2007

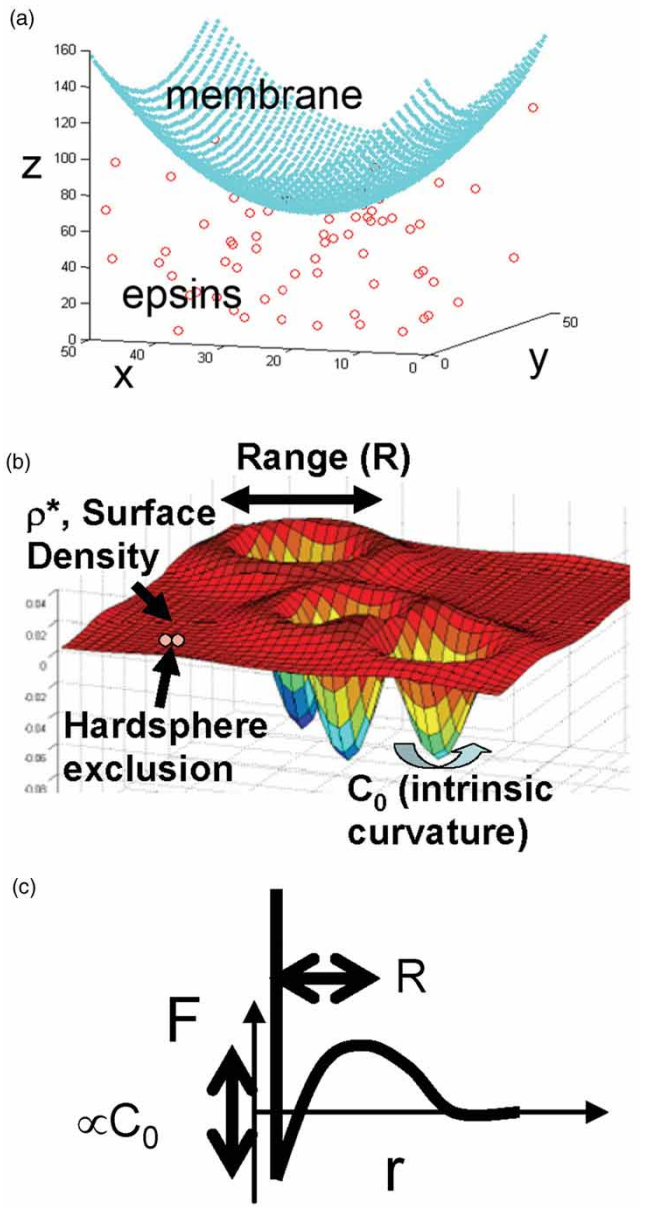

Figure 1. Model: (a) depiction of the system; (b) protein–membrane interaction parameters; (c) form of the potential of mean force between two adsorbed epsins.

kinetic Monte Carlo (KMC) scheme [41] on a discretized grid ('lattice') in which each hop (diffusion) to a neighbouring lattice site is treated as an elementary chemical reaction with a rate inversely proportional to the time-scale of diffusion. Proteins can freely diffuse in the extracellular or intracellular space and adsorb/desorb on the membrane (see figure 1(a)). The association, dissociation constants and the intracellular/extracellular and lateral (membrane-bound) diffusion coefficients are available from the experimental data published in the literature [19, 43, 44]. For the diffusible species, the rate of hopping k to a neighbouring 'lattice site' is determined as $k = D/a_0^2$, where D is the diffusion coefficient and a_0 is the lattice spacing. The KMC simulations are carried out such that the acceptance rates for the reactions conform to the Gillespie probability distribution [41], see below.

Every KMC move is considered as a chemical reaction $R_\mu\,(\mu = 1, \ldots, M)$ characterized by its stochastic rate constant c_μ, such that $c_\mu\,\mathrm{d}t$ gives the average probability that the particular move R_μ will take place in the next infinitesimal time interval $\mathrm{d}t$. For the set of diffusion moves we consider, there is a one-to-one correspondence between c_μ and the rate constant k. Given a particular state of the system at time t, the probability that a R_μ reaction will occur within the interval $(t, t + \Delta t)$ is $a_\mu\,\mathrm{d}t = h_\mu c_\mu\,\mathrm{d}t$, where h_μ is the number of distinct combinations for the reaction R_μ to occur; the above equality defines a_μ. With the above definitions, the reaction probability density function $P(\tau, \mu)$ is given by [41]:

$$P(\tau, \mu) = \begin{cases} a_\mu \exp(-a_T \tau), & \text{if } 0 \le \tau \le \infty, \\ 0, & \text{otherwise.} \end{cases} \tag{1}$$

Here, $a_T = \sum_i a_i$ and $P(\tau, \mu)\,\mathrm{d}\tau$ is the probability that, given the state at time t, the next reaction will occur in the infinitesimal time interval $(t + \tau, t + \tau + \mathrm{d}\tau)$ and will be a R_μ reaction.

In order to generate τ and μ according to the distribution specified in equation (1), we generate two random numbers r_1 and r_2 between 0 and 1 (end points excluded) from a unit-interval uniform distribution (0, 1) and set

$$\tau = (1/a_T)\ln(1/r_1), \tag{2}$$

and μ to be that integer for which

$$\sum_{\nu=1}^{\mu-1} a_\nu < r_2 a_T \le \sum_{\nu=1}^{\mu} a_\nu. \tag{3}$$

2.3. *Membrane dynamics*

The work of Helfrich in the 1970s permits a clean, curvilinear-free representation of 'thin' membranes, using the so-called Monge notation, where we use the Cartesian coordinates x, y, under the presumption that deformation is small relative to the axis normal to the surface [1, 5].

Localized membrane deformation and curvature is coupled with the adsorption of species on the membrane surface. Epsin induces a change in the intrinsic curvature of an otherwise planar membrane. The energy cost associated with membrane deformation is minimized by

Downloaded By: [University of Pennsylvania] At: 17:48 17 January 2007

the subsequent relaxation process occurring during membrane dynamics. This interaction formally establishes the coupling between membrane motion and diffusion of species interacting with the membrane. We describe the dynamics of the membrane via a time-dependent Ginzburg–Landau (TDGL) model (see Chakraborty and co-workers [19, 45–49])

$$\frac{\partial z}{\partial t} = -M\frac{\delta F}{\delta z} + \zeta, \tag{4}$$

where $z = z(x, y, t)$ is the distance of the deformed membrane segment from a reference plane (figure 1(a)), M is a generalized mobility factor associated with the membrane dynamics, ζ is the thermal noise term and F is the Helfrich free energy functional (in Monge or Cartesian notation) associated with membrane elasticity [1, 4, 5, 47]. F is given by [25],

$$F = \int\int \mathrm{d}x\,\mathrm{d}y \frac{1}{2}[(\gamma + \kappa C^2)(\nabla z)^2 + \kappa(\nabla^2 z - C)^2]. \tag{5}$$

Here, γ is the interfacial tension, κ is the bending rigidity and $C(x, y)$ is the intrinsic curvature. The values of κ, γ and M for a phospholipid bilayer membrane are obtained from experiments [19]: $\gamma = 3\,\mu\mathrm{N\,m^{-1}}$, $\kappa = 400 k_\mathrm{B}T$ and $M = 10^{-5}\,\mu\mathrm{m}^4/(k_\mathrm{B}T \cdot s)$. In the equation above, the integrand accounts for elastic energy associated with membrane bending and interfacial tension. The value of intrinsic curvature C is taken to be zero if no protein (epsin in our case) molecules are adsorbed and non-zero if the molecules are adsorbed. The above equation is solved numerically using a finite difference scheme for a given profile of $C(x, y)$ that is dictated by the adsorbed species and for a square patch of the membrane (1 μm in length with periodic boundary conditions in x and y dimensions), see appendix. The noise term is generated by drawing a random number from a Gaussian distribution with zero mean and with variance depending on T and the viscosity of the surrounding medium, (in our case this is assumed to be water). The finite difference equations (see appendix) are solved using MATLAB. The simulation results in a constant temperature dynamics for the membrane.

2.4. *Protein–membrane interaction*

Epsin is an amphiphilic moiety, with both hydrophilic and hydrophobic regions. The latter is in the form of an alpha-helix (helix 0), composed of leucine and isoleucine amino acid functional groups. Epsin's interaction with the bilayer membrane is intrinsically linked to the hydrophobicity of this region. The ability of epsin to modify the intrinsic curvature of bilayer membranes has been indirectly inferred from membrane tubulation studies [42]. The crystal structure of epsin's ENTH domain in the presence (i.e. bound to) and absence of the lipid head group inositol-1,4,5-trisphosphate (Ins(1,4,5)P3) shows that helix 0 becomes ordered at the N-terminus, upon binding to the lipid [42, 51]. It is also established that the protein behaves as a monomer, and that monomeric interactions cause changes in membrane curvature. Based on the experimental results of the tubulation study with wild-type and mutant proteins, it is hypothesized that helix zero is inserted into one leaflet of the lipid bilayer, thus inducing curvature. The current physical picture is that the insertion of helix 0 into the outer leaflet of the bilayer pushes the lipid head groups apart, thereby inducing curvature in the membrane. According to this hypothesis, the lateral expansion of surface area of lipid membranes upon the inclusion of epsin given by $(A_\mathrm{l} - A_\mathrm{l,o})/A_\mathrm{l,o}$ (A_l is the area per lipid molecule in the presence of epsin, and $A_\mathrm{l,o}$ is that in the absence of epsin) will drive the curvature induction on the membrane due to the difference in the degrees of area expansion in the inner and outer leaflets of the bilayer membrane. The bilayer membrane, therefore, assumes a curvature in order to topologically accommodate this difference.

Localized in the vicinity of an adsorbed epsin, the membrane is assumed to have an intrinsic curvature $C(x, y)$ as depicted in figure 1(b). The form of this localized function is assumed to be Gaussian with a range R and a magnitude C_0; the adsorbed epsins are charted as smooth Gaussians, with peak (maximum) values set to be C_0 with units μ^{-1}. C_0 scales as $1/\Re$, $\Re$ being the characteristic radius of curvature, see section 3.1. While a range of R and C_0 values are explored in our simulations, the exact values for a particular system (i.e. specific protein adsorbing on a membrane) can be calculated using fully atomistic simulations as well as measured in the experiments (see section 4).

2.5. *Multiscale model integration (integration of diffusion and membrane dynamics)*

We are concerned with the consequences of proteins (epsins) inducing membrane curvature and thereby dictating the dynamics of the system. The proteins themselves are diffusing; therefore our model explicitly maps a set of probabilistic events (namely diffusion) onto the deterministic one, namely that of a membrane deformation over discrete time-steps. This comprises the bulk of our present integration of separate time-scales.

Based on a scaling analysis, we have determined that the choice of integration depends on the competition between time-scales of diffusion and membrane motion.

Downloaded By: [University of Pennsylvania] At: 17:48 17 January 2007

The relevant time-scales are a_0^2/D (diffusion of the protein species) and $C_0^2 a_0^4/M$ (membrane motion). Depending on the Deborah number, $De = (a_0^2/D)/(C_0^2 a_0^4/M)$, two regimes will be of relevance: (1) adiabatic limit: the diffusion occurs much faster than membrane deformation ($De \ll 1$); (2) nonadiabatic limit: $De \sim 1$, the diffusion happens at similar time-scales to that of membrane dynamics. In the adiabatic limit, we determine the steady state profiles $C(x, y)$ (determined via epsin positions on the membrane in the KMC simulations) at every time-step of integration involving the membrane dynamics (TDGL) equations. In this limit, since the behaviour of the membrane largely occurs on a far longer time-scale than protein diffusion events, we compute time averages of the protein dynamics from the diffusion part of our algorithm and feed these time-averaged quantities to the algorithm which deals with membrane deformation. Our results described in this paper outline the system's dynamic behaviour in the adiabatic limit. First, we consider the variational problem and then discuss its numerical implementation (see appendix) within the finite difference scheme.

2.6. *The variational problem*

We solve the variational problem posed in equation 4 in order to determine the time-evolution of membrane height $z(x, y)$ via functional differentiation; the term $z(x, y)$ is augmented by $\epsilon\eta(x, y)$, ϵ being a small scalar increment and η being an arbitrary function with a boundary value and gradient of zero as x and y approach $\pm\infty$. We compute the derivative of the integrand with respect to ϵ at its infinitesimal limit:

$$\begin{aligned}
\frac{\delta F}{\delta z} &= \frac{\mathrm{d}}{\mathrm{d}\eta}\left\{\int\int_A \mathrm{d}x\,\mathrm{d}y \frac{1}{2}\frac{\mathrm{d}}{\mathrm{d}\epsilon}\left[\left(\gamma+\kappa C^2\right)(\nabla(z+\epsilon\eta))^2\right.\right.\\
&\quad \left.\left.+\kappa\left(\nabla^2(z+\epsilon\eta)-C\right)^2\right]_{\epsilon=0}\right\}\\
&= \frac{\mathrm{d}}{\mathrm{d}\eta}\int\int_A \mathrm{d}x\,\mathrm{d}y\left[\left(\gamma+\kappa C^2\right)\nabla(z+\epsilon\eta)\cdot\frac{\mathrm{d}}{\mathrm{d}\epsilon}\nabla(z+\epsilon\eta)\right.\\
&\quad \left.+\kappa\left(\nabla^2(z+\epsilon\eta)-C\right)\frac{\mathrm{d}}{\mathrm{d}\epsilon}\left(\nabla^2(z+\epsilon\eta)-C\right)\right]_{\epsilon=0}\\
&= \frac{\mathrm{d}}{\mathrm{d}\eta}\int\int_A \mathrm{d}x\,\mathrm{d}y\left[\left(\gamma+\kappa C^2\right)(\nabla z+\epsilon\nabla\eta)\cdot\nabla\eta\right.\\
&\quad \left.+\kappa\left(\nabla^2 z+\epsilon\nabla^2\eta-C\right)\left(\nabla^2\eta\right)\right]_{\epsilon=0}\\
&= \frac{\mathrm{d}}{\mathrm{d}\eta}\int\int_A \mathrm{d}x\,\mathrm{d}y\left[\left(\gamma+\kappa C^2\right)(\nabla z)\cdot\nabla\eta+\kappa\left(\nabla^2 z-C\right)\left(\nabla^2\eta\right)\right].
\end{aligned}$$

We solve these two parts separately. Letting $f(x, y) = \gamma + \kappa C^2$,

$$\begin{aligned}
f(x,y)\nabla z\cdot\nabla\eta &= f(x,y)\nabla\cdot(\eta\nabla z)-\eta f(x,y)\nabla^2 z\\
&= \nabla\cdot(f(x,y)\eta\nabla z)-\eta\nabla z\cdot\nabla f(x,y))\\
&\quad -\eta f(x,y)-\eta f(x,y)\nabla^2 z\\
&= \nabla\cdot(\eta\ldots)-\eta\left(\nabla z\cdot\nabla f(x,y)+f(x,y)\nabla^2 z\right).
\end{aligned}$$

Therefore, $(\gamma+\kappa C^2)(\nabla z)\cdot\nabla\eta = \nabla\cdot(\eta\ldots)-\eta(2\kappa C\nabla z\cdot\nabla C+(\gamma+\kappa C^2)\nabla^2 z)$.

Next, letting $g(x, y) = \nabla^2 z - C$,

$$\begin{aligned}
\kappa g(x,y)\nabla^2\eta &= \kappa[\nabla\cdot(g(x,y)\nabla\eta)-\nabla g(x,y)\cdot\nabla\eta]\\
&= \kappa\left[\nabla\cdot(g(x,y)\nabla\eta)-\nabla\cdot(\eta\nabla g(x,y)\right.\\
&\quad \left.+\eta\nabla^2 g(x,y)\right]\\
&= \kappa\left[\nabla\cdot(g(x,y)\nabla\eta-\eta\nabla g(x,y))+\eta\nabla^2 g(x,y)\right].
\end{aligned}$$

Therefore, $(\nabla^2 z - C)(\kappa\nabla^2\eta) = \kappa\nabla\cdot(\nabla\eta(\nabla^2 z - C) - \eta\nabla(\nabla^2 z - C)) + \eta\kappa\nabla^2(\nabla^2 z - C)$.

In both of the above cases, the volume integration of the divergence term becomes a surface integral at infinity of a zero-valued function (due to the properties of η), and the latter terms which are multiplied by η become the solutions to the variational problem. These yield

$$-M\frac{\delta F}{\delta z} = M\kappa\left(2C\nabla z\cdot\nabla C+\left(\frac{\gamma}{\kappa}+C^2\right)\nabla^2 z-\nabla^2\left(\nabla^2 z-C\right)\right),$$

from which we get,

$$\frac{1}{M\kappa}\frac{\partial z}{\partial t} = 2C\nabla z\cdot\nabla C+\left(\frac{\gamma}{\kappa}+C^2\right)\nabla^2 z-\nabla^4 z+\nabla^2 C,$$

where $\nabla^4 = \nabla\cdot\nabla(\nabla^2) = \partial_{xxxx}+\partial_{yyyy}+2\partial_{xxyy}$. More explicitly,

$$\begin{aligned}
\frac{1}{M\kappa}z_t &= 2C\left(z_x C_x+z_y C_y\right)+\left(\frac{\gamma}{\kappa}+C^2\right)\left(z_{xx}+z_{yy}\right)\\
&\quad -\left(z_{xxxx}+z_{yyyy}+2z_{xxyy}\right)+\left(C_{xx}+C_{yy}\right). \qquad (6)
\end{aligned}$$

We can furthermore derive such an equation for the intrinsic curvature, which is also straightforward. Starting with the same free energy integral as before,

Downloaded By: [University of Pennsylvania] At: 17:48 17 January 2007

we get

$$\begin{aligned}\frac{\delta F}{\delta C} &= \frac{\mathrm{d}}{\mathrm{d}\eta}\int\int_A \frac{\mathrm{d}x\,\mathrm{d}y}{2}\frac{\mathrm{d}}{\mathrm{d}\epsilon}\Big[\big(\gamma+\kappa(C+\epsilon\eta)^2\big)(\nabla z)^2 \\ &\quad +\kappa\big(\nabla^2 z-(C+\epsilon\eta)\big)^2\Big]_{\epsilon=0} \\ &= \frac{\mathrm{d}}{\mathrm{d}\eta}\int\int_A \mathrm{d}x\,\mathrm{d}y\big[\eta\kappa C(\nabla z)^2-\eta\kappa\big(\nabla^2 z-C\big)\big] \\ &= C\kappa\big((\nabla z)^2+1\big)-\kappa\nabla^2 z,\end{aligned}$$

which gives

$$\frac{\delta F}{\delta C} = C\kappa\big((\nabla z)^2+1\big)-\kappa\nabla^2 z. \tag{7}$$

From these we may interpret how adsorbed proteins are conducive to long-range interaction. Since the above variational derivative is itself a scalar field defined along the membrane surface, we may define another scalar field simultaneously, $\Delta C(x,y)$, governing the change of intrinsic curvature (or adsorbed protein concentration) experienced by the the membrane for a given diffusion decision made by a protein. If we begin to discuss each protein as carrying along with it some local curvature field function, we may regard these as the characteristic basis functions comprising $\Delta C(x,y)$.

3. Results

3.1. *Criticality of intrinsic curvature*

An important property of membrane-mediated epsin–epsin interaction that we would like to capture within the scope of our model is an effective attraction—resulting from a convexity in free energy as a function of radial distance—that would drive spontaneous aggregation (and hence favouring the tendency for vesicle formation). To explore its origin, we may regard equation (7) as defining an effective 'conservative' force for membrane mediated epsin–epsin attraction. This idealizes our multiscale KMC-TDGL scenario, since it avoids all considerations of thermal (Brownian) behaviour. To focus on the equilibrium point of a two-epsin system, we recast our free energy functional in the format of a 'central-force' description, keeping one epsin fixed and allowing an approaching epsin to interact with it via the membrane mediated generalized force. Let $f(r)$ be the radial force. From equation (7) we have

$$\begin{aligned}\mathbf{f}(\mathbf{r}) &= -\frac{\partial F}{\partial|\mathbf{r}|} = -\int\int_A \frac{\delta F}{\delta C}\frac{\mathrm{d}C(x,y)}{\mathrm{d}r}\,\mathrm{d}x\,\mathrm{d}y \\ &= -\int\int_A \big(C(x,y)\kappa\big((\nabla z)^2+1\big)-\kappa\nabla^2 z\big)\frac{\mathrm{d}C(x,y)}{\mathrm{d}r}\,\mathrm{d}x\,\mathrm{d}y.\end{aligned} \tag{8}$$

We note that $C(x,y)$ is explicitly dependent on the locations of the two epsins under consideration, and in-turn depends on their distance, $|\mathbf{r}|$, from one another. Equation (8) allows us to write,

$$\begin{aligned}\mathbf{f}(\mathbf{r}) = &-\frac{\kappa}{2}\frac{\mathrm{d}}{\mathrm{d}r}\int\int_A C^2\big((\nabla z)^2+1\big)\,\mathrm{d}x\,\mathrm{d}y \\ &+\frac{\mathrm{d}}{\mathrm{d}r}\int\int_A C\kappa\nabla^2 z\,\mathrm{d}x\,\mathrm{d}y.\end{aligned} \tag{9}$$

Then integrating along the radial distance r_1 to another, r_2, we get the energy change experienced by an epsin relocated from some radial position r_1 relative to the *stationary* epsin to the new position r_2, again relative to the stationary epsin,

$$\begin{aligned}\Delta U(|\mathbf{r}|=r_1\to r_2) &= \int_{r_1}^{r_2}\mathbf{f}(\mathbf{r})\cdot(d\mathbf{r}) \\ &= \frac{\kappa}{2}\left[\int\int_A C^2\big((\nabla z)^2+1\big)\,\mathrm{d}x\,\mathrm{d}y\right]_{|\mathbf{r}|=r_1}^{|\mathbf{r}|=r_2} \\ &\quad -\left[\int\int_A C\kappa\nabla^2 z\,\mathrm{d}x\,\mathrm{d}y\right]_{|\mathbf{r}|=r_1}^{|\mathbf{r}|=r_2}.\end{aligned} \tag{10}$$

We extend our analytic treatment further by assuming that the induced curvature is radially symmetric so that the standard association of C_0 with two characteristic radii $(\Re_1,\Re_2)$ of deformation given by $C_0=(1/\Re_1+1/\Re_2)$; instead we write $C_0=2/\Re$. Now assuming that the functional form of C for the ith epsin is a delta function, centred about the epsin's centre (neglecting steric exclusion for the time being),

$$\begin{aligned}C_i(x,y) &\equiv \frac{2}{\Re}\,\delta(|\mathbf{r}-\mathbf{r}_i|), \\ C_i(x,y)^2 &\equiv \frac{4}{\Re^2}\,\delta(|\mathbf{r}-\mathbf{r}_i|).\end{aligned}$$

Then equation (10) gives us the relation

$$\Delta U(|\mathbf{r}|=r_1\to r_2) = \frac{2\kappa}{\Re}\left[\frac{1}{\rho}(\nabla z)^2-\nabla^2 z\right]_{|\mathbf{r}|=r_1}^{|\mathbf{r}|=r_2}.$$

The implied transition between energetically favourable and energetically unfavourable nucleation landscapes is intuitive: a smaller induced curvature ($\Re\to\infty$) allows for a region of greater convexity in the membrane to 'pull' an epsin in. Meanwhile, any increase at all in the concavity of membrane height will cause epsin–epsin repulsion.

Downloaded By: [University of Pennsylvania] At: 17:48 17 January 2007

3.2. *Manifestation of protein–membrane interaction*

In extending the above discussion to the model discussed in section 2, it is first instructive to examine the relationship between the lattice diffusion of proteins and the continuum dynamics of the membrane in the adiabatic limit. Since there is a clear separation of time-scale in this case, the KMC steps are carried out for approximately $\Delta t/(a_0^2/D_i)$ steps, where Δt is the time step of integration for the TDGL equations. The KMC moves alter the epsin coordinates and in turn the $C(x, y)$ function. This is how the KMC moves affect the TDGL dynamics of the membrane. The presence of two adsorbed proteins on the membrane introduces an energy landscape for the lateral diffusion of epsins on the membrane. This has its origin from the $\delta F/\delta C$ term producing a Ginzburg–Landau equation of the form [37]:

$$\frac{\partial C}{\partial t} = -\tilde{M}\frac{\delta F}{\delta C} + \zeta \Rightarrow \frac{\Delta C}{\Delta t} \sim \frac{\Delta C}{a_0^2/D}\frac{\delta F}{\delta C}.$$

We derived the second relationship based on a simple scaling analysis to illustrate the fact that the time-scale of lateral diffusion on the membrane has two components. The bare component is given by the a_0^2/D, and the generalized force component arising from the above equation is given by the $\delta F/\delta C$ term. Hence, the time-scale for lateral diffusion is given by $[a_0^2/D_i]/[\delta F/\delta C]$. This in turn renormalizes the rate constants used in the KMC moves. Therefore, it is evident that even in the adiabatic limit, the membrane dynamics affect KMC moves. In our simulations, we perform this renormalization of kinetic constants for each KMC move on-the-fly as dictated by the membrane conformation.

The physical picture emerging from these interactions is that the renormalized interaction between two epsin molecules (the so-called potential of mean force) has the form as depicted in figure 1(c), where F is the effective free energy and r is the distance between two adsorbed epsins. The exact form of this potential depends on the values of the hard-sphere exclusion, γ, κ, R and C_0. The form of $F(r)$ implies the following: (1) the system is dominated by repulsion at two length scales, the exclusion diameter and the point outside the exclusion diameter where $F(r)$ is maximized (see section 3.4). These interactions are likely to conspire in inducing order (or spatial correlations) in adsorbed epsins analogous to the ordering in a two-dimensional liquid; (2) that there is a barrier in localizing the epsin molecules in a region on the membrane, which depends on the height where $F(r)$ is maximized, and therefore on R and C_0 as well. The barrier has to be overcome (as in a nucleation event) before the epsins can collectively act to curve the membrane.

3.3. *Dynamical behaviour of protein-adsorbed membranes*

We are now poised to present the results from the successful application of the KMC-TDGL multiscale method for the case of epsin adsorbing on phospholipid membranes (there are no other proteins present in the system). In order to obtain the state and dynamical behaviour associated with the protein-adsorbed membrane phase, we explore a range of values for the parameters ρ^*, C_0 and R, while holding γ, κ, M and T fixed. A depiction of our findings from a series of multiscale simulations for different sets of interaction parameters is provided in figure 2; in these pictures, the protein positions are omitted, blue regions correspond to recessed and red correspond to elevated parts of the membrane.

For $R = 40\,\text{nm}$ ($R^* = 2$, twice the epsin diameter) and $C_0 = 20\,\mu\text{m}^{-1}$, the protein–membrane interaction is weak and the induced curvature is much localized around the epsin positions (1st and 2nd rows, figure 2). Increasing ρ^* does not affect this local behaviour. Thus, for small values of R and C_0, vesicle nucleation is likely absent for any value of ρ^*. For $R = 60\,\text{nm}$ and $C_0 = 10\,\mu\text{m}^{-1}$, the dynamics is similar to that described above (3rd row, figure 2), but for values of $C_0 > 40\,\mu\text{m}^{-1}$, membrane invagination is observed (contrast 3rd–5th rows of figure 2). This event is non-cooperative and occurs even at low ρ^*, due to the large curvature induced by each individual protein. At $R = 80\,\text{nm}$, sub-threshold values of $C_0 < 30\,\mu\text{m}^{-1}$, and small ρ^*, we observe no nucleation (6th row); but, as we increase ρ^*, we observe membrane invagination arising from cooperative fluctuations (compare rows 6 and 7 in figure 2). The cooperativity manifests as a persistence of spatial and orientational correlations among the epsins (discussed in section 3.4) and is also marked by epsin localization. However, in our simulation, the membrane invagination was not stable (and therefore subsided) for long times, indicating the formation of a subcritical nucleus. This nucleus was stabilized for long times when the range R was increased to 100 nm (row 8, figure 2) and the nucleation led to long-time membrane invagination.

3.4. *Liquid-like structuring of epsins adsorbed onto the membrane*

In figure 2, we reported protein-mediated membrane dynamical behaviour for a range of physical parameters. In order to further characterize the state of the system as a function of these parameters, we quantify the spatial organization and temporal responses of the system by introducing several correlation functions. The spatial organization of the adsorbed proteins on the membrane

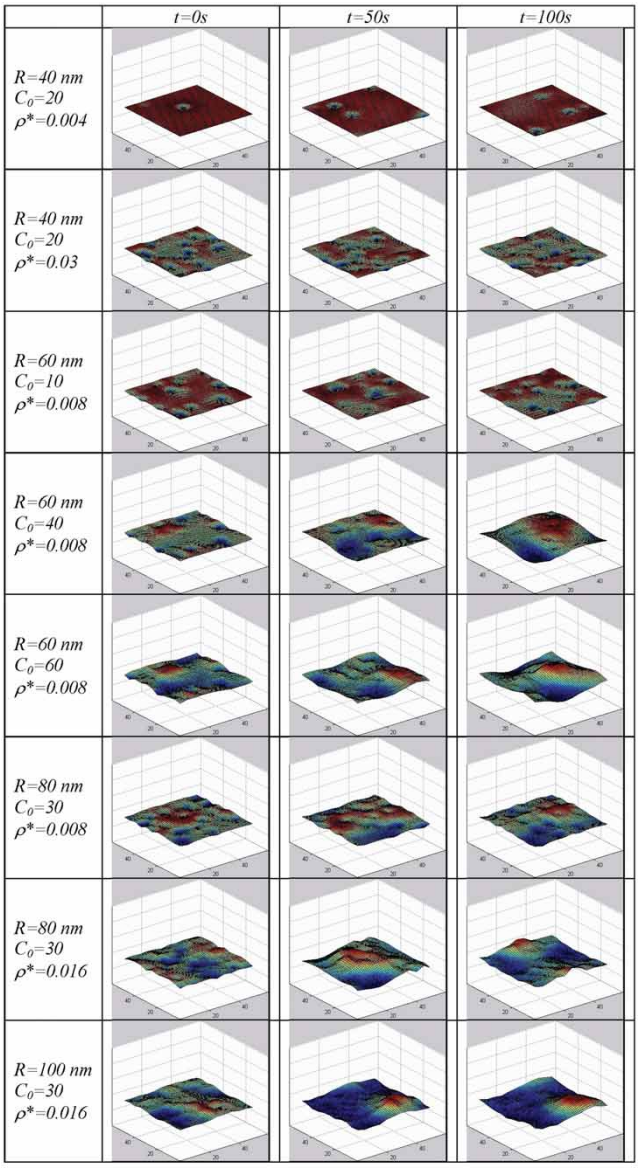

Figure 2. Snapshots depicting the behaviour of the protein-adsorbed membrane for different sets of model parameters. For each parameter set, a time course is obtained from the simulations from which three snapshots are depicted. For clarity, only the membrane is shown, (the epsin positions are omitted). Blue regions correspond to recessed, and red regions to elevated parts of the membrane.

is recorded by calculating the radial distribution function $g(r) = \rho^*(r)/\langle\rho^*\rangle$, where the quantity in the numerator is the surface density of adsorbed proteins at a particular location and that in the denominator is its spatial average. Going by the form of the potential mean force in figure 1(c), we expect to see correlations between proteins at two length scales, namely, the hard-sphere exclusion and the range of interaction, R. Radial distribution functions for different states of the protein–membrane system provided in figure 3(a) are reminiscent of those for a 2-dimensional fluid with the repulsive interaction (packing) dictated by the value of R rather than the exclusion distance. At low density, the radial distribution function for small values of R resembles that of a dilute hard-sphere system in two dimensions. For larger values of R and at higher densities, significant spatial correlations are present. In particular, the non-zero values of $g(r)$ for $r < R$ signifies the co-localization of epsin molecules on the membrane. The free energy landscape associated with such a co-localization can be inferred from the potential of mean force $f(r) = -k_B T \ln g(r)$.

A closely associated characteristic spatial quantity is the orientational correlation function $\langle\Psi_6^*(0)\Psi_6(r)\rangle$, where $\Psi_6(r)$ is given by $\sum_j \exp[\mathrm{i}6\theta_j(r)]$. Here, $\mathrm{i} = \sqrt{-1}$, the index j runs from 1 to the number of nearest neighbours to any given protein at location r, and $\theta_i(r)$ is the angle formed by the projection of the line joining the nearest neighbours to any given protein at location r, and $\theta_i(r)$ is the angle formed by the projection of the line joining the nearest neighbours (termed as nearest neighbour bond) on the xy plane with the x axis. Nearest neighbour pairs are identified as those pairs of molecules that are separated by a distance that falls in the range of the first peak of the $g(r)$ function. The quantity $\langle\Psi_6^*(0)\Psi_6(r)\rangle$, therefore, measures the persistence of bond-orientational correlations (or hexagonal ordering) among the membrane-adsorbed proteins (figure 3(b)). Our results show that the persistance of orientational correlation occurs for $R > 80\,\mathrm{nm}$, $C_0 > 20\,\mu\mathrm{m}^{-1}$ and $\rho^* > 0.016$. Taken together with the occurrence of membrane invagination, we deduce that under these conditions, the orientational correlations cause cooperative fluctuations among epsins to drive nucleation.

In order to track the dynamical response of the system, we introduce two temporal correlation functions. The first is the membrane height autocorrelation function $\langle\sigma_z(0)\sigma_z(t)\rangle$, where $\sigma_z(t)$ is the standard deviation of the height of the membrane at each spatial location (if averaged everywhere, the height is always zero) at time t. This membrane height autocorrelation function is sensitive to any global rearrangement in membrane geometry and yields the relaxation time associated with such reorganization (figure 3(c)). In the figure, the correlation functions under several conditions show a diverse relaxation behaviour. The functions' transition between two plateau values, the magnitude of the difference signifies the amplitude associated with the membrane relaxation, and the time taken for the transition signifies the corresponding relaxation time. The relaxation times span several orders of magnitude indicating the importance of protein mediation in membrane dynamics. In particular, the long relaxation time indicated by $\times$ is a reflection of a glassy behaviour.

Downloaded By: [University of Pennsylvania] At: 17:48 17 January 2007

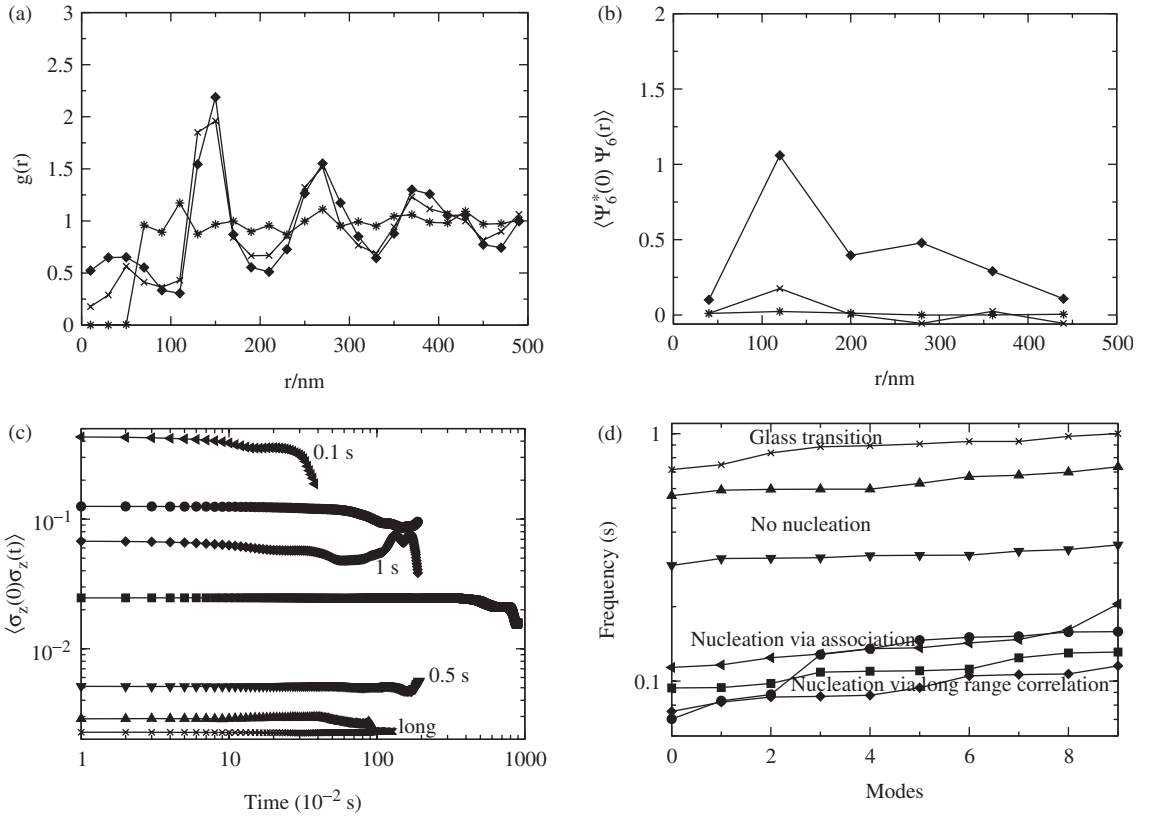

Figure 3. Correlation functions: (a) radial distribution functions showing liquid-like order with packing determined by the range R; (b) orientational correlation functions showing persistence of correlations for up to $4R$; (c) height correlation functions showing the relaxation time associated with the dominant membrane undulation mode; (d) frequency spectrum indicating the time-scales for different dynamical behaviour. The symbols correspond to: $*$ $R = 40$ nm, $C_0 = 20$, $\rho^* = 0.004$; $\lhd$ $R = 60$ nm, $C_0 = 60$, $\rho^* = 0.008$; ∇ $R = 40$nm, $C_0 = 20$, $\rho^* = 0.003$; $\square$ $R = 80$ nm, $C_0 = 30$, $\rho^* = 0.016$; $\bigcirc$ $R = 100$ nm, $C_0 = 30$, $\rho^* = 0.016$; $\times$ $R = 80$ nm, $C_0 = 5$, $\rho^* = 0.02$; $\triangle$ $R = 80$ nm, $C_0 = 20$, $\rho^* = 0.03$; $\diamond$ $R = 80$ nm, $C_0 = 10$, $\rho^* = 0.02$.

Regimes where cooperative spatial and orientational correlations persist also show slower dynamical response.

In addition to the membrane height autocorrelation, we calculate the frequency spectrum of the membrane undulations using principal component analysis [49] and quasiharmonic analysis. We calculate the covariance matrix of height fluctuations $\tilde{H}$ (the tilde representing a matrix here) in Cartesian space whose elements are given by: $H_{ij} = \langle (z_i - \langle z_i \rangle)(z_i - \langle z_i \rangle)^{\mathrm{T}} \rangle$, where i and j run from $1, \ldots, N$, N being the total number of grid points resolving the membrane, z represents the height in the Cartesian system of coordinates and the superscript 'T' denotes transpose. Diagonalization of $\tilde{H}$ yields eigenvalues and eigenvectors corresponding to the principal modes, which represent a set of independent directions of membrane undulation modes (the principal components). The normalized magnitude of the corresponding eigenvalue is a measure of amplitudes of the undulation along the eigenvector. The first few eigenvalues (in decreasing order) describe the largest height fluctuations. Within the quasi-harmonic approximation [50, 51] (which is based on the equipartition of energy among different dynamical modes of undulation), the frequency ν_i associated with the ith undulating mode is given by $\nu_i = (1/2\pi)(k_{\mathrm{B}}T/e\nu_i)^{1/2}$, where $e(\nu_{iv})$ is the eigenvalue of the corresponding mode. The frequency spectra associated with membrane dynamics in figure 2 are provided in figure 3(d). In addition to the dominant membrane relaxation modes, the frequency response also depicts the time-scales associated with other membrane undulation modes. Again, a diverse set of temporal responses are observed for the different conditions.

4. Discussion and conclusions

The development of the KMC-TDGL methodology in the adiabatic limit (where there is a clear separation of time-scales) and its application to the case of protein-mediated membranes is illustrated. Even in the adiabatic limit, there is coupling between the lattice and continuum degrees of freedom through the energy landscape. This coupling is unique to the problem considered here because the lattice dynamics and the

Downloaded By: [University of Pennsylvania] At: 17:48 17 January 2007

Downloaded By: [University of Pennsylvania] At: 17:48 17 January 2007

continuum dynamics occur in the same spatial domain. To be specific, the protein diffusion determines the intrinsic curvature function $C(x, y)$ for membrane dynamics and the membrane curvature, in-turn, presents an energy landscape for protein diffusion. To account for this coupling correctly, the updates of the intrinsic curvature function $C(x, y)$ and the rate constants associated with KMC moves are performed on-the-fly.

We applied the KMC-TDGL method to a protein adsorbed membrane system in order to determine the influence of protein–membrane interaction and protein concentration on the phase and dynamic behaviour of the membrane. Our findings can be summarized as follows: for small values of R and C_0, we observe no nucleation at any value of ρ^*. For intermediate values of R, above a threshold value of $C_0 = 40\,\mu\mathrm{M}^{-1}$, we observe membrane invagination. This event was, however, non-cooperative and occurred even at low ρ^*, solely due to the large curvature induced by each protein. At intermediate values of R and sub-threshold values of C_0 and moderately high ρ^*, we observed nucleation followed by membrane invagination due to cooperative fluctuations. This was marked by epsin localization, just as one would expect in an endocytotic internalization event. The spatial and dynamical correlations provide us with the measures necessary for a comprehensive thermodynamic and dynamic characterization of (and therefore measures to distinguish between) the different states of the protein–membrane system. For example, the persistence of spatial and orientational correlation is a signature of cooperative behaviour. Moreover, dynamical correlations yield membrane relaxation times which reflect on the dynamical state of the system (liquid versus glass). Therefore, by exploring the range of values of R and C_0, different states with markedly different equilibrium and dynamic behaviour were identified.

Our mesoscopic method is based on simplified physical models and model parameters, which enable the bridging of disparate length scales, but nevertheless introduce approximations. The functional form and the specific values of the interactions in our multiscale model can be validated by independently calculating them in microscopic simulations or measuring them experimentally. For example, within fully atomistic, explicit water molecular dynamics simulations, a reliable route to estimating the elastic constants in microscopic simulations is to employ the cell method of Yoshimoto and co-workers [55] and calculate the stress tensor σ_{ij} directly from dynamics trajectories [55–57]. For the membrane system, the interfacial tension γ is obtained by integrating over the stress profile; namely, $\gamma = \int \mathrm{d}z[\sigma_{zz} - (\sigma_{xx} + \sigma_{yy})/2]$ [18, 58]. Decomposition of the elastic moduli into the renormalized elastic constant κ appearing in the Helfrich free energy function equation (5) is cumbersome. Instead, it is possible to estimate this parameter through fluctuation relationships. Following Lipowsky and co-workers [55], this can be achieved by computing the fluctuation spectrum $S(q) = \langle |z(q)|^2 \rangle$, where $z(q)$ is the Fourier transform of $z(r)$. A fit to the scaling of the $S(q) \sim k_\mathrm{B}T/\kappa q^4 + k_\mathrm{B}T/\gamma q^2$ will yield the estimation of the parameter κ. Finally, the value of the intrinsic curvature C_0 can be calculated by integrating over the lateral stress profile, $\sigma_\parallel = \sigma_{xx}$ and using the relationship: $2\kappa C_0 = \int z\left[\partial\sigma_\parallel/\partial z\right]\mathrm{d}z$ [59]. Independent measurements of these parameters (namely, interfacial tension and bending rigidity) from experiments are also possible [19, 60].

Several predictions from our modelling of the protein–membrane dynamics can be directly tested in experiments: the calculated values of relaxation times in figure 3 can be compared with those obtained from dielectric relaxation spectroscopy measurements on protein-adsorbed membranes [61–65]. Parameters such as interfacial tension and bending rigidity can be measured using micropipette experiments and local deformation/curvature can be measured using confocal microscopy and X-ray diffraction. These experiments provide avenues to validate model predictions.

Several extensions to our multiscale approach can be made to make it more general and widely applicable. In the regime where the time-scales overlap ($De \sim 1$), the discrete (KMC) process has to be integrated with the continuous TDGL equations. One possible route to achieving this integration is in the spirit of surface hopping methodology introduced by Tully and co-workers [65, 66]. Our methodology can also be extended to include a curvilinear representation allowing for larger deformations, and hydrodynamic interactions between adsorbed epsins if detailed calculations of the potential of mean force is available through atomistic simulations. These avenues will be pursued in future studies. We note that even though our efforts are focused on membrane mediated processes, the proposed multiscale strategy is general enough to be applicable to many problems requiring the integration of lattice and continuum length scales; examples include biochemical signal transduction, DNA dynamics and DNA–protein interactions, and crystal growth, to name a few.

Acknowledgements

This work constituted J. Weinstein's Senior Undergraduate Project in the Department of Physics at The University of Pennsylvania. We thank Dr Mark Goulian for numerous discussions on this subject and for pointing us towards many references in the literature. We thank Dr Charlie Epstein for discussions on the

numerical stability of the finite difference scheme. Funding for this work was partially available by a grant from the Whitaker Foundation.

Appendix: Numerical analysis of the membrane finite difference equations

Our intent is to transcribe our fourth-order differential equation into a difference equation in x and y. The first-order time derivative we represent as a back-difference between the times m and $m-1$, or

$$\phi_{i,j}^{m} = \phi_{i,j}^{m-1} + \phi_{i,j}^{(1)}\tau + \frac{\phi_{i,j}^{(2)}\tau^2}{2} + \cdots,$$
$$\phi_{i,j}^{(1)}\tau = \left[\frac{\phi_{i,j}^{m} - \phi_{i,j}^{m-1}}{\tau}\right] + O(\tau),$$

where (i, j) indexes the x–y lattice coordinates and $\phi = \phi(x, y, t)$ designates the arbitrary single-valued function under consideration. Similarly, in one spatial dimension, taking the Taylor expansion about $i+1$ and subtracting it from the corresponding expansion about $i-1$ we get

$$\phi_i^{(1)} = \frac{\phi_{i+1} - \phi_{i-1}}{2\epsilon} - \frac{\epsilon^2\phi_i^{(3)}}{3!} + O(\epsilon^4).$$

Similarly, adding the two we get

$$\phi_i^{(2)} = \frac{\phi_{i+1} - 2\phi_i + \phi_{i-1}}{\epsilon^2} - \frac{2\epsilon^2\phi_i^{(4)}}{4!} + O(\epsilon^2).$$

There are two methods worth addressing in solving for the highest-order terms: iteration of the second-order difference equation and a derivation from the bottom up, using linear combinations of Taylor expansions to systematically minimize error. Were we to iterate the above, we would inherit a recursive definition of the fourth-order derivative evaluated at neighbouring points. We therefore choose the latter, combining Taylor expansions for neighbouring spaces on a 1D grid, $i+1$, $i+2$, $i-1$ and $i-2$. For some linear combination encoded in the matrix A:

$$\begin{pmatrix} \phi_{i+1} - \phi_i \\ \phi_{i+2} - \phi_i \\ \phi_{i-1} - \phi_i \\ \phi_{i-2} - \phi_i \end{pmatrix} = A \begin{pmatrix} \epsilon\phi^{(1)} \\ \epsilon^2\phi^{(2)} \\ \epsilon^3\phi^{(3)} \\ \epsilon^4\phi^{(4)} \\ \epsilon^5\phi^{(5)} \\ \epsilon^6\phi^{(6)} \end{pmatrix} + O(\epsilon^7).$$

We define A on a per-row basis.

$$A_{1,n} = \frac{1}{n!}, \quad A_{2,n} = \frac{2^n}{n!}, \quad A_{3,n} = \frac{(-1)^n}{n!}, \quad A_{4,n} = \frac{(-2)^n}{n!}.$$

This gives us 4 equations that correspond to the Taylor expansions at the 4 neighbouring points. Of these equations, we need a linear combination that eliminates all ϕ^n except $\phi^{(4)}$, which is the value for which we are solving. Then,

$$\frac{1}{n!}(a_1 + a_2(2)^n + a_3(-1)^n + a_4(-2)^n) = 0, \quad n \neq 4,$$

for some set of coefficients a_1, a_2, a_3 and a_4. Notice, however that we have 5 equations even if we exclude $n=4$. Therefore, the solution is over-determined. In order to solve this homogeneous equation, we must reduce the n's for which we are solving. Realizing that we can sacrifice $n=1$ and 2, already having finite differences with acceptable error for their respective order derivatives, we will solve the system of equations for $n=3$, 5 and 6 to give the values,

$$a_1 = -64, \quad a_2 = 1, \quad a_3 = -64, \quad a_4 = 1.$$

We use these factors in the linear equation:

$$\begin{pmatrix} \phi_{i+1} - \phi_i \\ \phi_{i+2} - \phi_i \\ \phi_{i-1} - \phi_i \\ \phi_{i-2} - \phi_i \end{pmatrix} = \begin{pmatrix} 1 & \frac{1}{2} & \frac{1}{3!} & \frac{1}{4!} & \frac{1}{5!} & \frac{1}{6!} \\ 2 & 2 & \frac{8}{3!} & \frac{16}{4!} & \frac{32}{5!} & \frac{64}{6!} \\ -1 & \frac{1}{2} & -\frac{1}{3!} & \frac{1}{4!} & -\frac{1}{5!} & \frac{1}{6!} \\ -2 & 2 & -\frac{8}{3!} & \frac{16}{4!} & -\frac{32}{5!} & \frac{64}{6!} \end{pmatrix} \times \begin{pmatrix} \epsilon\phi^{(1)} \\ \epsilon^2\phi^{(2)} \\ \epsilon^3\phi^{(3)} \\ \epsilon^4\phi^{(4)} \\ \epsilon^5\phi^{(5)} \\ \epsilon^6\phi^{(6)} \end{pmatrix},$$

to eliminate all unknown derivatives (and, incidentally, the first-order derivative as well) to give $-64(\phi_{i+1} - \phi_i) + (\phi_{i+2} - \phi_i) - 64(\phi_{i-1} - \phi_i) + (\phi_{i-2} - \phi_i) = -60\epsilon^2\phi^{(2)} - 4\epsilon^4\phi^{(4)}$. Substituting in for $\phi^{(2)}$ its corresponding Taylor expansion through its sixth-order term, we get

$$\phi^{(4)} = \frac{\phi_{1-2} - 4\phi_{i-2} + 6\phi_i - 4\phi_{i+1} + \phi_{i+2}}{\epsilon^4 - \frac{\epsilon^2}{6}\phi^{(6)}|_i + 0(\epsilon^4)}.$$

Downloaded By: [University of Pennsylvania] At: 17:48 17 January 2007

Downloaded By: [University of Pennsylvania] At: 17:48 17 January 2007

While obtaining the cross term ϕ_{xxyy}, we do not need to go through the trouble of formulating the matrix problem because the iterative use of fourth-derivatives is one into which we can insert the above answer in...

$$\begin{aligned}\phi_{xxyy}|_{i,j} = \frac{1}{\epsilon^4}\Big\{&(\phi_{i-1}-2\phi_i+\phi_{i+1})_{j-1}-2(\phi_{i-1}-2\phi_i+\phi_{i+1})_j\\&+(\phi_{i-1}-2\phi_i+\phi_{i+1})_{j+1}\Big\}\\&-\frac{1}{12}(\phi_{xxxx}|_{i,j-1}-2\phi_{xxxx}|_{i,j}+\phi_{xxxx}|_{i,j+1})+O(\epsilon^2).\end{aligned}$$

x and y with some asymmetry. However, we can confide in the fact that any inaccuracy will emerge only in terms with $\epsilon^{n\geq 2}$.

We now rewrite equation (6) in terms of a finite difference, ensuring stability by the standard Crank–Nicholson method [68] (that is, applying a two-part time average to all derivatives of order greater than two). Cumulatively, with terms corresponding to the two time points m and $m-1$ separated, our equation becomes:

$$\begin{aligned}\frac{1}{M\kappa\tau}z^m_{i,j}-\frac{1}{2}\left\{\begin{array}{c}\frac{1}{\epsilon^2}\left(\frac{\gamma}{\kappa}+C^2_{i,j}\right)\left[\left(z^m_{i-1}-2z^m_i+z^m_{i+1}\right)_j+\left(z^m_{j-1}-2z^m_j+z^m_{j+1}\right)_i\right]\\-\frac{1}{\epsilon^4}\left[\begin{array}{c}\left(z^m_{i-2}-4z^m_{i-1}+6z^m_i-4z^m_{i+1}+z^m_{i+2}\right)_j\\+\left(z^m_{j-2}-4z^m_{j-1}+6z^m_j-4z^m_{j+1}+z^m_{j+2}\right)_i\end{array}\right]\\-2\cdot\frac{1}{12\epsilon^4}\left[\begin{array}{c}\left(-z^m_{i-2}+16z^m_{i-1}-30z^m_i+16z^m_{i+1}-z^m_{i+2}\right)_{j-1}\\-2\left(-z^m_{i-2}+16z^m_{i-1}-30z^m_i+16z^m_{i+1}-z^m_{i+2}\right)_j\\+\left(-z^m_{i-2}+16z^m_{i-1}-30z^m_i+16z^m_{i+1}-z^m_{i+2}\right)_{j+1}\end{array}\right]+O(\epsilon^2)\end{array}\right\}+O(\tau)\\=\frac{1}{M\kappa\tau}z^{m-1}_{i,j}+\frac{1}{2}\left\{\begin{array}{c}\frac{1}{\epsilon^2}\left(\frac{\gamma}{\kappa}+C^2_{i,j}\right)\left[\left(z^{m-1}_{i-1}-2z^{m-1}_i+z^{m-1}_{i+1}\right)_j+\left(z^{m-1}_{j-1}-2z^{m-1}_j+z^{m-1}_{j+1}\right)_i\right]\\-\frac{1}{\epsilon^4}\left[\begin{array}{c}\left(z^{m-1}_{i-2}-4z^{m-1}_{i-1}+6z^{m-1}_i-4z^{m-1}_{i+1}+z^{m-1}_{i+2}\right)_j\\+\left(z^{m-1}_{j-2}-4z^{m-1}_{j-1}+6z^{m-1}_j-4z^{m-1}_{j+1}+z^{m-1}_{j+2}\right)_i\end{array}\right]\\-2\cdot\frac{1}{12\epsilon^4}\left[\begin{array}{c}\left(-z^{m-1}_{i-2}+16z^{m-1}_{i-1}-30z^{m-1}_i+16z^{m-1}_{i+1}-z^{m-1}_{i+2}\right)_{j-1}\\-2\left(-z^{m-1}_{i-2}+16z^{m-1}_{i-1}-30z^{m-1}_i+16z^{m-1}_{i+1}-z^{m-1}_{i+2}\right)_j\\+\left(-z^{m-1}_{i-2}+16z^{m-1}_{i-1}-30z^{m-1}_i+16z^{m-1}_{i+1}-z^{m-1}_{i+2}\right)_{j+1}\end{array}\right]+O(\epsilon^2)\end{array}\right\}\\+2C_{i,j}\cdot\frac{1}{(2\epsilon)^2}\left[\left(z^{m-1}_{i+1}-z^{m-1}_{i-1}\right)_j(C_{i+1}-Ci-1)_j+\left(z^{m-1}_{j+1}-z^{m-1}_{j-1}\right)_i\left(C_{j+1}-C_{j-1}\right)_i\right]\\+\frac{1}{\epsilon^2}\left[(C_{i-1}-2C_i+C_{i+1})_j+\left(C_{j-1}-2C_j+C_{j+1}\right)_i\right].\end{aligned}$$

This expands to

$$\begin{aligned}\phi_{xxyy}|_{i,j} = &\frac{\left(\begin{array}{c}(-\phi_{i-2}+16\phi_{i-1}-30\phi_i+16\phi_{i+1}-\phi_{i+2})_{j-1}\\-2(-\phi_{i-2}+16\phi_{i-1}-30\phi_i+16\phi_{i+1}-\phi_{i+2})_j\\+(-\phi_{i-2}+16\phi_{i-1}-30\phi_i+16\phi_{i+1}-\phi_{i+2})_{j+1}\end{array}\right)}{12\epsilon^4}\\&+O(\epsilon^2).\end{aligned}\tag{11}$$

Note that because it depends on the order we plug in variables x and y into equation (6), equation (11) treats

Arithmetic aside, we are ready to insert these coefficients into the linear problem $Az|_m = Bz|_{m-1} + R$ for which, given a time step τ and curvature distribution $C(x, y)$, we can compute the discrete time evolution of the membrane.

Stability, however, remains of immediate interest. The Courant–Friedrich–Levy (CFL) condition [69] dictates that any propagation in a space interval corresponding to ϵ which projects a causal change over a time interval τ must be governed by some invariant—a 'light cone', so to speak—for which the physical domain of causality

does not outpace the numerical domain of causality. In our case, we may see simply by inspection from equation (6) that the highest order time and space terms preserve the scaling relationship $1/M\kappa\tau \sim 1/\epsilon^4$. CFL therefore conditions our solution to the regime where $\tau < \epsilon^4/M\kappa$. Any discretization that does not obey this rule must necessarily be unstable.

In order to satisfy CFL, two separate grids were constructed for dealing with epsin diffusion and membrane deformation, the former fine, the latter coarse, taking as input from a time-weighted average interpolated from the former. Adsorbed epsins were charted as smooth Gaussians, with peak (maximum) values set to be C_0 with units μ^{-1}. (C_0 scales as $1/\Re$, $\Re$ being the characteristic radius of curvature, see section 3.1).

Downloaded By: [University of Pennsylvania] At: 17:48 17 January 2007

References

[1] D. R. Nelson, T. Piran, and S. Weinberg, *Statistical Mechanics of Membranes and Surfaces: jerusalem Winter School for Theoretical Physics, Jerusalem, 28 Dec. 87–6 Jan. 88* (World Scientific, Singapore, Teaneck, NJ, 1989).

[2] P. M. Chaikin and T. C. Lubensky, *Principles of Condensed Matter Physics* (Cambridge University Press, Cambridge, New York, 1995) (includes bibliographical references and index).

[3] S. Komura and S. A. Safran, Europ. Phys. J. E **5,** 337 (2001).

[4] S. A. Safran, Adv. Phys. **48,** 395 (1999).

[5] D. R. Nelson, T. Piran, and S. Weinberg, *Statistical Mechanics of Membranes and Surfaces*, 2nd ed. (World Scientific, River Edge, NJ, 2004.

[6] V. Degiorgio and M. Corti, *Physics of Amphiphiles–Micelles, Vesicles, and Microemulsions, 1983: Varenna on Lake Como, Villa Monastero, 19–29 July 1983* (North-Holland Pub. Co., Amsterdam, New York, 1985).

[7] S. A. Pandit, D. Bostick, and M. L. Berkowitz, Biophys. J. **85,** 3120 (2003).

[8] G. R. Pradhan, S. A. Pandit, A. D. Gangal, and V. Sitaramam, J. Theor. Biol. **220,** 189 (2003).

[9] S. J. Marrink and A. E. Mark, Biophys. J. **87,** 3894 (2004).

[10] M. L. Berkowitz, D. L. Bostick, and S. Pandit, Chem. Rev. **106,** 1527 (2006).

[11] S. Izvekov, A. Violi, and G. A. Voth, J. Phys. Chem. B **109,** 17019 (2005).

[12] S. J. Marrink and A. E. Mark, Biophys. J. **88,** 384A (2005).

[13] A. P. Alivisatos, P. F. Barbara, A. W. Castleman, J. Chang, D. A. Dixon, M. L. Klein, G. L. McLendon, J. S. Miller, M. A. Ratner, P. J. Rossky, S. I. Stupp, and M. E. Thompson, Adv. Mater. **10,** 1297 (1998).

[14] L. Saiz, S. Bandyopadhyay, and M. L. Klein, Biosci. Rep. **22,** 151 (2002).

[15] G. A. Khelashvili, S. A. Pandit, and H. L. Scott, J. Chem. Phys. **123,** 34910 (2005).

[16] M. Schick, K. Katsov, and M. Mueller, Biophys. J. **88,** 66A (2005).

[17] M. Schick, M. Mueller, and K. Katsov, Biophys. J. **82,** 543A (2002).

[18] S. J. Marrink and A. E. Mark, J. Phys. Chem. B **105,** 6122 (2001).

[19] S. E.Lee, Y. Hori, J. T. Groves, M. L. Dustin, and A. K.Chakraborty, Trends Immunol. **23,** 500 (2002).

[20] T. R. Weikl, R. R. Netz, and R. Lipowsky, Phys. Rev. E **62,** R45 (2000).

[21] T. R. Weikl and R. Lipowsky, Phys. Rev. E **6401,** 1 (2001).

[22] T. R. Weikl, J. T. Groves, and R. Lipowsky, Europhys. Lett. **59,** 916 (2002).

[23] Z. G. Wang and S. A. Safran, Europhys. Lett. **11,** 425 (1990).

[24] V. Nikolov, R. Lipowsky, H. G. Dobereiner, and R. Dimova, Biophys. J. **86,** 197A (2004).

[25] E. J. Wallace, N. M. Hooper, and P. D. Olmstead, Biophys. J. **88,** 4072 (2005).

[26] P. B. S. Kumar, G. Gompper, and R. Lipowsky, Phys. Rev. Lett. **86,** 3911 (2001).

[27] F. L. Brown, Biophys. J. **84,** 842 (2003).

[28] S. L. Veatch and S. L. Keller, Phys. Rev. Lett. **89,** 1 (2002).

[29] T. Baumgart, S. Das, W. W. Webb, and J. T. Jenkins, Biophys. J. **89,** 1067 (2005).

[30] A. Radhakrishnan and H. McConnell, Proc. Natl. Acad. Sci. USA **102,** 12662 (2005).

[31] D. Vlachos, Adv. Chem. Eng., **30**, 1 (2005).

[32] M. Kirkham and R. G. Parton, Biochim. Biophys. Acta **1746**, 349 (2005).

[33] R. G. Parton, M. Hanzal-Bayer, and J. F. Hancock, J. Cell Sci. **119,** 787 (2006).

[34] A. A. Schmidt, Nature **419,** 347 (2002).

[35] W. N. E. B. Engquist and Z. Y. Huang, Phys. Rev. B **67,** 1 (2003).

[36] D. C. Wylie, Y. Hori, A. R. Dinner, and A. K. Chakraborty, J. Phys. Chem. B, **110**, 12749 (2006).

[37] B. K. Dey, H. Rabitz, and A. Askar, J. Chem. Phys. **119**, 5379 (2003).

[38] J. Liu, S. Qi, J. T. Groves, and A. K. Chakraborty, J. Phys. Chem. B. **109**, 19960 (2005).

[39] L. Hinrichsen, A. Meyerholz, S. Groos, and E. J. Ungewickell, PNAS **103,** 8715 (2006).

[40] P. C. Hohenberg and B. I. Halperin, Rev. Mod. Phys. **49**, 435 (1977).

[41] D. T. Gillespie, J. Phys. Chem. **81,** 2340 (1977).

[42] M. G. J. Ford, I. G. Mills, Y. Vallis, G. J. K. Praefcke, P. R. Evans, and H. T. McMahon, Nature **419,** 361 (2002).

[43] Y. C. Fung, *Biomechanics: Circulation* (Springer-Verlag, New York, 1997).

[44] G. Bell, M. Dembo, and P. Bongrand, Biophys. J. **45,** 1051 (1984).

[45] A. K. Chakraborty, Nature Immunol. **3,** 895 (2002).

[46] A. K. Chakraborty, Sci. Stke **122,** PE10 (2002).

[47] S. J. Lee, Y. Hori, J. T. Groves, M. L. Dustin, and A. K. Chakraborty, Trends Immunol. **23,** 492 (2002).

[48] K. H. Lee, A. R. Dinner, C. Tu, G. Campi, S. Raychaudhuri, R. Varma, T. N. Sims, W. R. Burack, H. Wu, J. Wang, O. Kanagawa, M. Markiewicz, P. M. Allen, M. L. Dustin, A. K. Chakraborty, and A. S. Shaw, Science **302,** 1218 (2003).

[49] S. J. Lee, Y. Hori, and A. K. Chakraborty, Proc. Natl. Acad. Sci. USA **100,** 4383 (2003).

[50] S. A. Safran, Surf. Sci. **500,** 127 (2002).

[51] R. V. Stahelin, F. Long, B. J. Peter, D. Murray, P. De Camilli, H. T. McMahon, and W. Cho, J. Biol. Chem. **278,** 28993 (2003).
[52] M. A. Balsera, W. Wriggers, Y. Oono, and K. Schulten, J. Phys. Chem. **100,** 2567 (1996).
[53] I. Andricioaei and M. Karplus, J. Chem. Phys. **115,** 6289 (2001).
[54] R. M. Levy, M. Karplus, J. Kushick, and D. Perahia, Macromolecules, **17,** 1370 (1983).
[55] K. Yoshimoto, T. S. Jain, P. F. Nealey, and J. J. de Pablo, J. Chem. Phys. **122,** 1 (2005).
[56] K. Yoshimoto, T. S. Jain, K. V. Workum, P. F. Nealey, and J. J. de Pablo, Phys. Rev. Lett. **93,** 1 (2004).
[57] G. J. Papakonstantopoulos, K. Yoshimoto, M. Doxastakis, P. F. Nealey, and J. J. de Pablo, Phys. Rev. E **72,** 1 (2005).
[58] R Goet, G. Gompper, and R. Lipowsky, Phys. Rev. Lett. **82,** 221 (1999).
[59] D. Marsh, Biophys. J. **81,** 2154 (2001).
[60] Z. Chen and R. P. Rand, Biophys. J. **73,** 267 (1997).
[61] M. Naumowicz and Z. A. Figaszewski, Biophys. J. **89,** 3174 (2005).
[62] M. Naumowicz and Z. A. Figaszewski, J. Membr. Biol. **205**, 29 (2005).
[63] A. D. Petelska, M. Naumowicz, and Z. A. Figaszewski, Bioelectrochemistry **65,** 143 (2005).
[64] A. D. Petelska, M. Naumowicz, and Z. A. Figaszewski, Colloids Surf. B Biointerfaces **44,** 158 (2005).
[65] M. Naumowicz, J. Kotynska, A. Petelska, and Z. Figaszewski, Eur. Biophys. J. **35,** 239 (2006).
[66] S. Hammes-Shiffer and J. C. Tully, J. Chem. Phys. **103**, 8528 (1995).
[67] L. J. LaBerge and J. C. Tully, Chem. Phys. **260,** 183 (2000).
[68] J. Crank and P. Nicolson, Proc. Cambridge Phil. Soc. **43**, 50 (1947).
[69] R. Courant, K. Friedric and H. Lewy, IBM J. Res. Develop. **11,** 215 (1967).

Downloaded By: [University of Pennsylvania] At: 17:48 17 January 2007